Pre-Main Sequence Objects and Star Formation Efficiency in Dark Clouds within Taurus Complex

AUTHOR(S):

Kim, Chil Yeong

CITATION:

Kim, Chil Yeong. Pre-Main Sequence Objects and Star Formation Efficiency in Dark Clouds within Taurus Complex. Memoirs of the Faculty of Science, Kyoto University. Series of physics, astrophysics, geophysics and chemistry 1990, 38(1): 1-23

ISSUE DATE:

1990-03

URL:

http://hdl.handle.net/2433/257612

Memoirs of the Faculty of Science, Kyoto University, Series of Physics, Astrophysics, Geophysics and Chemistry, Vol. XXXVIII, No. 1, Article 1, 1990

Pre-Main Sequence Objects and Star Formation Efficiency in Dark Clouds within Taurus Complex

By

Chil Yeong KIM

Department of Physics, Faculty of Science, Kyoto University

(*Received December 25, 1988*)

Abstract

Using the 1 m telescope of Agematsu Infrared Observatory, we have carried out an infrared (J, K) survey in three dense portions of the Taurus dark cloud complex, and detected 328 sources in total. For each source detected in the survey, we also conducted a photometry in the J, H, and K bands. A discrimination between pre-main sequence objects and field stars was attempted in a two color (J–H, H–K) diagram. From the analysis of our survey together with the IRAS survey, 27 pre-main sequence (PMS) candidates have been newly identified, which increases the amount of stellar mass in the clouds significantly. The cloud mass in the survey regions was estimated from extinction of the field stars. We derived the mass ratios of PMS objects to the clouds to be 5–6% for all these clumps. These values are slightly larger than previously estimated ones but still far smaller than the lower limit to make a gravitationally bound stellar system. The star formation in the Taurus dark cloud complex appears to form unbound stellar groups.

Key words: near-infrared survey; pre-main sequence objects; star formation efficiency.

1. Introduction

The efficiency of star formation provides us an important clue to understand the evolution of molecular clouds. A number of searches for pre-main-sequence (PMS) objects have been made to estimate the efficiency in dark cloud complexes in the optical and infrared regions. In order to estimate the efficiency strictly, one should find out all of the PMS objects in a cloud. There are various types of objects in the category of PMS objects (see Sects. 2). Although there are many means of observation capable of detecting some types, none of them are effective for all the types of PMS objects. In order to find out all of the PMS objects in a cloud, one should perform various kinds of observations. The efficiency, however, was roughly estimated on the basis of specified types of PMS objects so far.

The Taurus dark cloud complex contains many small clouds (Fig. 1) and numerous T Tauri stars (Cohen and Kuhi 1979), which indicate that this is a region of recent star formation. The distance to this complex was determined to be roughly 140 pc (Elias 1978c). The galactic longitude and latitude are about 170° and −12°. Gilmore (1980) found no evidence for the formation of massive stars in a radio continuum search. This complex has good conditions to study the spontaneous formation of low-mass stars: proximity, small contamination by field stars, and paucity of massive stars. A large

number of investigations to find out the various kinds of PMS objects have been made in this complex (see Sect. 2). A near-infrared (NIR) survey in this complex was already made by Elias (1978c), but it was not enough to reveal embedded PMS objects because its limiting magnitude was too low, about 7.5 mag in the K band (see Sect. 6.1). In fact, a number of PMS objects known from the optical observation were not detected in his survey. In order to reestimate the star formation efficiency including all the types of PMS objects in this complex, we attempted to make a deeper NIR survey at least enough to detect all of the known PMS objects.

In this paper we present an investigation to estimate the star formation efficiency in three clouds within the Taurus dark cloud complex. In order to find out moderately obscured objects we have carried out a NIR survey to 9.5mag in the K band, deep enough to detect the majority of the PMS objects except heavily obscured objects. For all the sources detected in the survey we have made a JHK photometry, which is useful for the discrimination of the PMS objects from field stars and the estimation of the mass of the clouds. In addition, we have compiled heavily obscured objects from the analysis of the infrared astronomical satellite (IRAS) survey as well as the already known PMS objects.

An introduction to the PMS objects is given in Sect. 2; the observations and results are presented in Sect. 3; an identification of the PMS objects is given in Sect. 4; a derivation of the cloud mass and an estimation of the star formation efficiency are described in Sect. 5; and some discussions are given in Sect. 6.

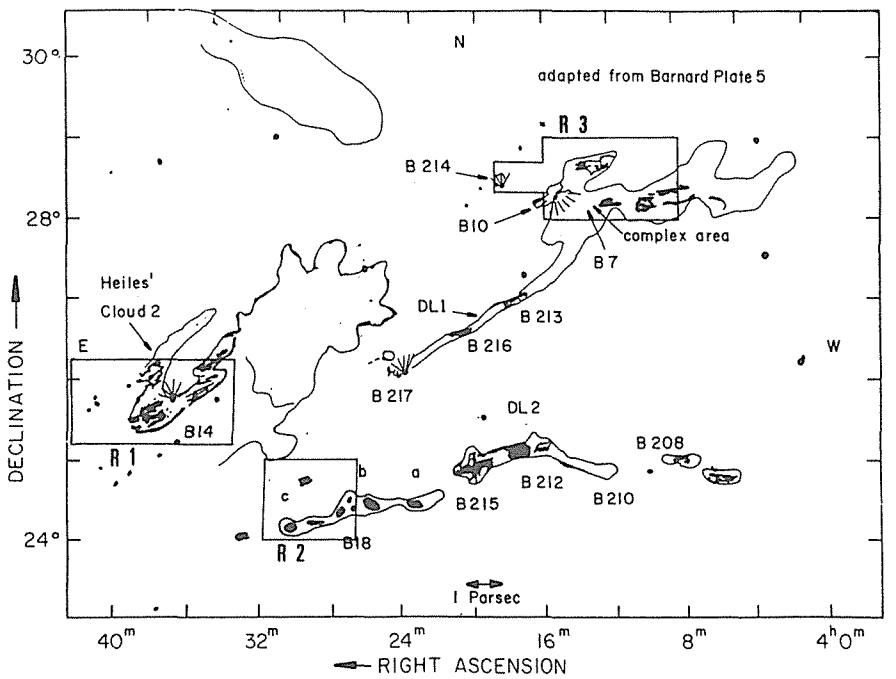

Figure 1 The survey regions, superposed on a schematic map of the Taurus dark cloud complex from Clark, Giguere, and Crutcher (1977).

2. Pre-main sequence objects

A star is born in the dense region of clouds and evolves into a normal main sequence star through the pre-main sequence (PMS) phase, along an evolutionary track (Hayashi 1961; 1966). Hereafter we will use the term of the PMS objects for all the young stellar objects which have not arrived yet at the zero age main sequence (ZAMS). In the first stage of the evolution, the PMS objects are generally surrounded with thick circurmstellar matter of low temperature. They emit most of the radiation in the far-infrared (FIR) region. Next, many objects, if not all, develop bipolar outflows, which play a role to remove the circurmstellar matter. As the circurmstellar matter clears, the objects come to be visible in the near-infrared, and eventually in the optical region. They are usually characterized with infrared excess (Rydgren and Vrba 1983) and strong emission lines (Cohen and Kuhi). These features decline and eventually disappear as the objects approach the ZAMS (Lindroos 1986). The PMS objects show different properties with the proceeding of the evolution. They can be distinguished from normal main sequence stars by virtue of their variability, emission lines, and/or infrared excess. By means of observational properties, they may be divided into several groups; T-Tauri stars (TTSs), weak emission line stars (WELSs), and embedded objects identified with NIR or FIR observations. We will briefly describe the progress and present status of the observations to detect them.

The TTSs characterized by strong emission lines and variability (Rydgren *et al.* 1976) are the most easily observable kind of PMS object in the optical wavelength range. The Hα emission line survey using the objective prism attached to the Schmidt camera is a very useful method in detecting the TTSs in large area of the celestial sphere. Therefore, it can be said that almost all TTSs except for the embedded ones with considerable obscuration have been found out by the Hα emission line survey in the Taurus dark cloud complex (Herbig and Rao 1972; Cohen and Kuhi 1979).

The WELSs are thought to be a kind of PMS objects observed in the optical or X-ray ranges. Compared with the TTSs, they show only faint emission lines as an indication of PMS objects. Historically they were investigated with an aim to search for post-TTSs which have passed the T Tauri phase but have not yet arrived at the zero age main sequence (ZAMS). From the comparison of the evolution time scale of the post-TTSs to that of TTSs, it is likely that the number of them is comparable to the number of TTSs, if star formation proceeds over one or more Kelvin-Helmholtz contraction times (Herbig 1978). Various observations have been made to find them, such as the proper motion survey (Jones and Herbig 1979), the X-ray emission survey (Walter and Kuhi 1981; Feigelson and Kriss 1981), the deep-Hα emission line survey (Feigelson and Kriss 1983), and the CaII H and K emission line survey (Herbig, Vrba and Rydgren 1986). In spite of the previous efforts, only a few objects were discovered, and none of them were identified as the genuine post-TTS. Although the attempts to discover the post-TTSs failed, it became clear that there are some young objects of the same age as TTSs but showing extremely weak emission lines (Weaver 1985; Herbig, Vrba and Rydgren 1986). Accordingly, they are called as weak emission line stars (WELSs) instead of post-TTSs. Although it is very difficult to find out them because of

their rather vague properties, they should be taken into consideration in estimating the efficiency of the star formation. Fortunately, most of the weak emission line stars except obscured ones are already found out in the Taurus complex region.

It is naturally conceived that there must be a number of PMS objects entirely embedded within dark clouds, so that the optical methods can not make access to them. Since the extinction generally decreases with increasing wavelengths, infrared surveys provide a powerful tool to probe such obscured objects. In addition, the PMS objects generally have an intrinsic infrared excess (e.g. Mendoza 1966, 1968; Rydgren, Schmelz and Vrba 1982; Rucinski 1985), which gives a clue to discriminate them from normal stars (see Sect. 3.2). A NIR survey thus appears to be an easy and effective method to find out the embedded PMS objects that are obscured moderately. In the first stage, NIR mappings to reveal optically-obscured stellar clusters were made at rather limited areas (about 0.1 deg^2) of dark cloud complexes (e.g., Allen 1972; Grasdalen et al. 1973; Strom, Strom and Vrba 1976). Although such observations were powerful in the survey of densest regions to search for the heavily obscured objects and crowded sources, one could not apply the method for finding moderately obscured objects distributed over the entire region of dark clouds because of too much observing time. Elias (1978 b; c) made a NIR survey in order to find out the obscured high-luminosity objects over the complex, using a large beam size of 2' and sidereal rate. He showed that most of the objects (about 90%) detected in the large-area survey appear to be field stars. Subsequently, Hyland, Jones and Mitchell (1982) carried out a moderately deep NIR survey of the Chamaeleon dark cloud complex in a moderately large area (about 0.4 deg^2) corresponding to a small cloud within the complex. They proposed a method to discriminate PMS objects from field stars in a two-color (J–H, H–K) diagram. The detailed explanation of the method and application to our observation will be given in Sects. 3.2.

Mid- or far-infrared surveys are the most effective method to reveal heavily obscured stars and extremely cool objects. The typical stellar population of the former is embedded-TTSs and that of the latter is proto-stars in cloud cores (e.g., Beichman *et al.* 1986). They can be detected only in the infrared, especially by FIR observations. The infrared astronomical satellite (IRAS) survey with photometric bands at 12, 25, 60 and 100 μm (Neugebauer *et al.* 1984) is suitable to that purpose. In Sect. 4.3, the results obtained from the analysis of the IRAS database will be given.

A PMS object may be detected through one or more methods. The typical TTSs are generally detected in all the methods mentioned above, but there are some known TTSs without FIR excess enough to be detected in the IRAS survey. If such TTSs are moderately obscured by the intracloud matter, they might be identified only in the near-infrared. In addition to them, there are some kinds of objects identified in only one wavelength range; WELSs and heavily obscured objects. In order to find out the PMS objects completely, one shoud have the existence of them in mind. In Sect. 4 we will compile the PMS objects existing within the survey region.

3. Observations and results

3.1 Selection of the survey area

In order to investigate the star formation efficiency in active regions of the Taurus complex, we have selected three obscured regions containing a concentration of TTSs, in view of the fact that (a) the star formation occurs at densest regions, which generally appear to be obscured regions, (b) the concentration of TTSs is a vital indications of star formation region, and (c) unknown PMS objects are most likely to be located at obscured regions.

The survey regions, superimposed on the schematic map of the Taurus complex from Clark, Giguere and Crutcher (1977), are illustrated in Figure 1. The covered areas of the regions 1, 2, and 3 are, respectively, 2.04, 1.14, and 1.95 square degrees. The region 2 and 3 correspond to the Group IIa and I in Jones and Herbig (1979), respectively; the region 1 corresponds to the north-east part of Group II, which shows a slightly loose concentration.

The visual extinction maps obtained from star counts (Fig. 1-d, f, g in Cernicharo, Bachiller and Duvert 1985) represent the optical appearance of the regions well. The region 1 containing the Heiles cloud 2 (Heiles 1968), which has been thought to be a favorable star formation site, appears to be the densest in the complex but contains only four previously-known PMS objects. Since only a few PMS objects have been known, one should expect many unknown embedded PMS objects. In contrast to the region 1, the region 2 centered on Barnard 18 appears to be less dense but contains many known PMS objects. It is interesting to compare the two regions in a viewpoint of star formation efficiency. The region 3 containing complex area appears to be moderately dense and contains several PMS objects, and therefore it is regarded as a region with intermediate properties between the region 1 and 2.

3.2 Near-infrared survey

The NIR survey was carried out by using the 1m infrared telescope at the Agematsu Infrared Observatory (AIRO) of Kyoto University during the observing seasons from 1983 to 1985. The observations were made with the two-channel InSb detector system, called "Futago", operated at a solid nitrogen temperature of about 55 K (Nakajima *et al.* 1985). In the observations, channels are assigned to the 1.25 μm (J) band and the 2.25 μm (K) band, whose band-passes are 0.38 and 0.48 μm respectively.

A scan was made with a rectangular field of $25'' \times 65''$ (RA, Dec) along right ascension at the sidereal rate by stopping the telescope tracking. Each scan was spaced by $30''$ apart in declination. The signal and the reference beams were separated by $90''$ in a direction of right ascension with the chopping secondary. Therefore, an infrared source should be detected more than four times: two times in the same scan and more than two times in the adjacent scans in declination.

In the present survey we have detected 131, 80, and 117 objects either in the K or J band, in the region 1, 2, and 3 respectively. The error of the positions obtained from scan data was about $25''$ in right ascension and $30''$ in declination. On the infrared plates ($\lambda_{\text{eff}}=7900$A; $\Delta\lambda=1800$A) taken with the 105 cm Kiso Schmidt telescope, we

identified each object detected in the survey with the brightest star within the error box ($25'' \times 30''$) and measured the position of it. Plate 1, 2, and 3 show the identification of them to the stars. Those objects are listed in Appendix 1, together with the position measured on the plate, with an accuracy of about $0.6''$. For the objects not identified in the plate, the positions were subsequently improved during the photometric observations, whose accuracy is about $5''$ both in right ascension and declination.

Figure 2 shows the histograms of K-mag distribution for the sources detected in each region, which peak in the range of 9.0–9.5 mag and then fall off rapidly. The minimum detectable signals corresponding to the 3σ noise level were 12 mag in the J band and 11 mag in the K band. It is clear that the detection probability is lower for the fainter sources. The limiting magnitude guaranteeing the complete detection in the present survey appears to be 9.5 mag in the K band. In the same way, that in the J band is 10.5 mag.

In Figure 2, solid lines show the numbers predicted from a galatic stellar distribution model (Jones *et al.* 1981), which are normalized to each survey area. Each survey region has a significant excess in number of stars in the range of 7.0–8.5 mag, that is, number of detection are larger than those predicted by the model. It can be explained by the contribution of PMS objects in the stellar population. Detailed discussion will be given in Sect. 4.2.

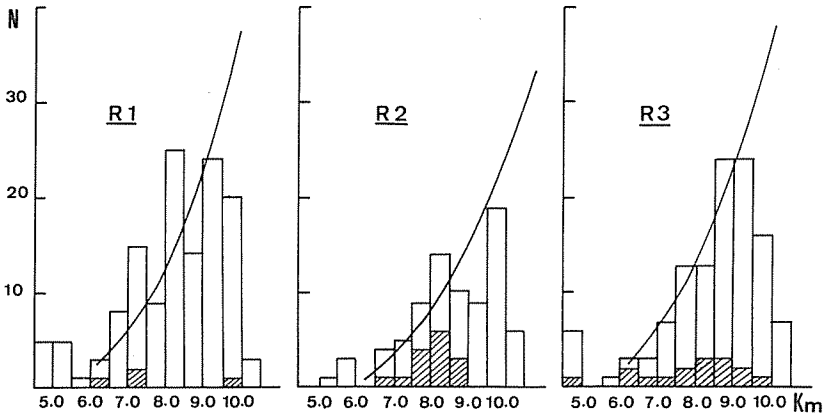

Figure 2 Histrograms of K-mag distributions for the sources detected in each region. Solid curves show the numbers predicted from the exponential disk model of Jones et al. (1981). The hatched parts denote the previously-known PMS object in the survey regions.

3.3 Near-infrared photometry

For all the objects detected in the survey, we carried out J (1.25 μm), H (1.68 μm), and K (2.28 μm) photometry during the period of 1986 November to 1987 May. These observations were made by using the same telescope that was used in the survey, but with a different photometer, called "Zo". The detection limits of the photometry system were 13.5, 12.5, and 11.5 magnitudes respectively in the J, H, and K band. For most of the sources, a 3 mm ϕ diaphragm corresponding to a $36'' \phi$ field of view at the focal plane

was adopted, while a 2 mm ϕ diaphragm of 24″ ϕ was also used for close double sources. No discrepancy between the two sizes of the diaphragm was noticed in the actual observations.

The results of the photometry are given in Appendix 1. The internal accuracy of the observed magnitudes is less than 0.01 mag for the sources brighter than 8.0 mag, while it is about 0.03 mag for the other sources, at all band. In Sect. 4.2 we will attempt to discriminate the PMS objects from field stars with the two-color diagram (J–H, H–K) obtained from the photometry.

4. The pre-main sequence objects within the survey regions

4.1. The optical PMS objects

As a result of the extensive efforts so far done in the optical region in the Taurus complex, it appears that the PMS objects potentially detectable in those wavelengths had been found out completely. The known PMS objects in the survey regions to date (35 objects) are listed in Table A1, together with the references. All of them were detected in the present survey, and most of them were in fact identified as PMS objects in the two-color diagram (see Sect. 4.2). We will regard all of them as PMS objects though 7 objects of them are not located in the domain of PMS objects on the two-color diagram.

4.2. The PMS objects assigned by the near-infrared observation

Although a large number of sources were detected in the NIR survey, each of them is not necessarily a PMS object. Elias (1978a) showed that the majority of the NIR sources are field stars not associated with the cloud. Therefore, the discrimination between PMS objects and the field stars is most important in the study of star formation by NIR survey within dark clouds.

Elias (1978b; c) employed a method using NIR spectral features such as the CO absorption (2.3 μm) or the Brγ emission for the discrimination. It provides good results, but consumes so much observing time. Hyland (1980) suggested an alternative method using the two-color diagram of (J–H, H–K). Hyland, Jones and Mitchell (1982) attempted to apply the method in the investigation of the Chamaeleon dark cloud and showed that it was extremely efficient in the discrimination. Nakajima *et al.* (1986) confirmed the validity of the method and showed their basis of the following three points.

1) The interstellar reddening laws in the near-infrared is nearly normal at any place of the cloud. Practically no evidence of anomalous reddening are noticed in the Taurus complex (Elias 1978c; Cohen and Kuhi 1979; Vrba and Rydgren 1985).

2) The field stars detected in the NIR survey are mainly giant stars of spectral type of G8 or later, which have a maximum value in the spectral energy distribution in the H band.

3) The PMS objects intrinsically have a redder spectral energy distribution than that of normal stars of the same spectral type. In other words they have moderate infrared excesses, which shift the PMS objects to the right side in the diagram.

Figs. 3-1, 2, and 3 show the two-color diagrams for the objects listed in Table A1. The solid curves are the loci of the intrinsic colors of main sequence stars and giant stars (Koornneef 1983). The straight line shows a locus of G8 giant stars reddened by the cloud. Giant stars of spectral type of later than G8 will be located at the upper-left of the line. Of the sources detected in the survey, 47 objects are picked up as PMS candidates due to their location in the diagrams. Of the 47 objects, 28 are previously-known PMS objects and the rest are newly identified PMS candidates. On the other hand, there are some known PMS objects that can not be discriminated from the field stars in the diagram, where they are denoted by open square. The details of each source are given in Table A1, together with classification.

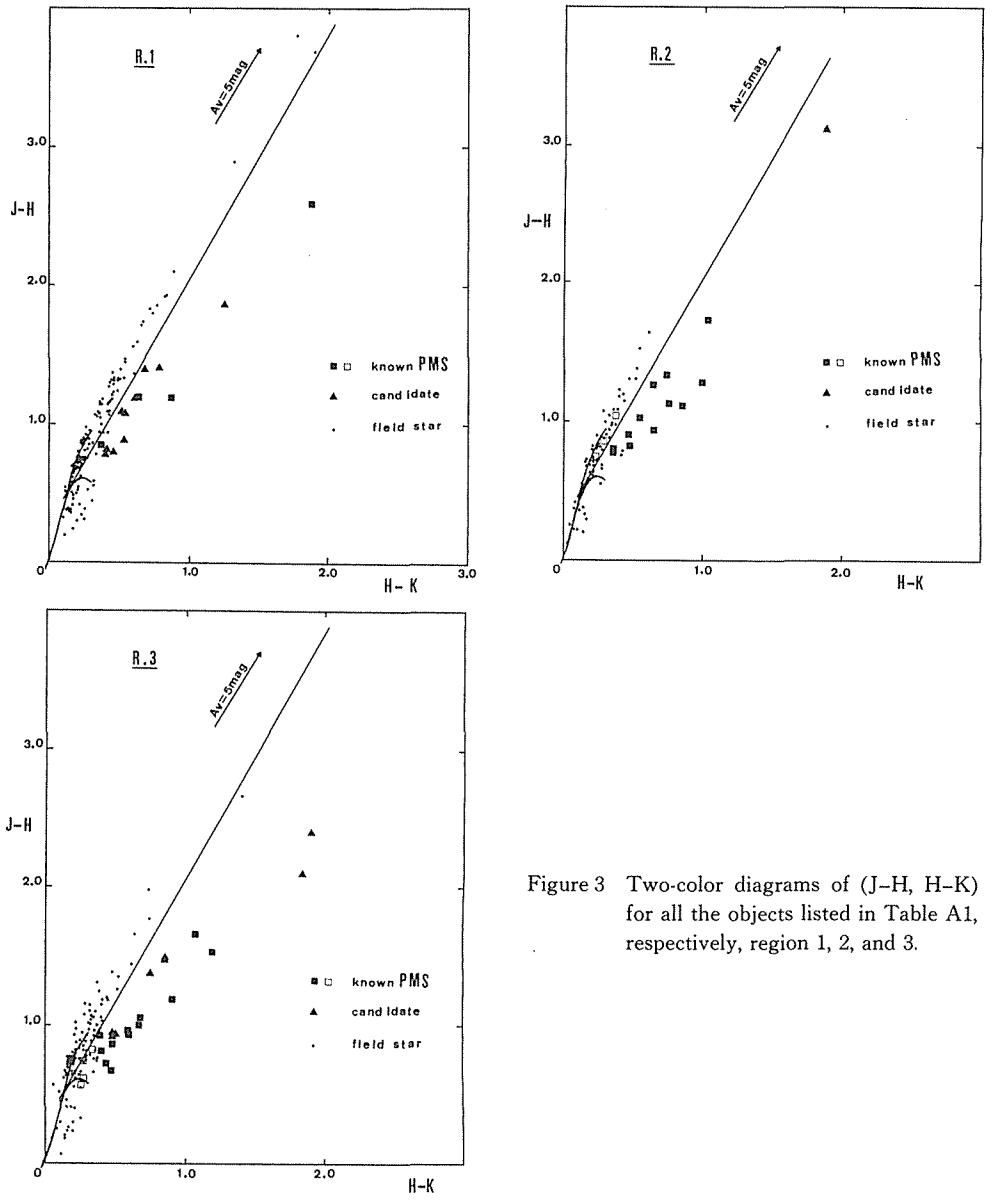

Figure 3 Two-color diagrams of (J-H, H-K) for all the objects listed in Table A1, respectively, region 1, 2, and 3.

4.3. The PMS objects detected in the IRAS survey

The results of the IRAS survey are useful to search for FIR excess stars and cool objects. From the Point Source Catalogue of the IRAS survey, we picked up the 65 sources detected at one or more bands in the present survey regions.

Beichman *et al.* (1986) show that IRAS objects can be classified into three kinds of objects from their location in the two-color diagram ([12]–[25], [25]–[60]); normal stars, FIR excess stars, and cool objects. Figure 4 shows the two color diagram of the IRAS sources detected in the 12, 25, and 60 μm band, which are classified into any of the groups above. For the remaining sources, we defined as the following; the sources undetected in the 25 and/or 60 μm band are normal stars, the sources undetected in the 12 and/or 25 μm band are cool objects, and the sources detected only in the 100 μm band are FIR cirri (cf., Beichman *et al.* 1984). Although the groups of FIR excess objects and cool objects also contain field sources such as peculiar stars and extra-galaxies, we have considered the groups to be associated objects with the cloud because they are located at the star formation region on the celestial sphere. The number density (per sq. degree) of the field sources is less than about 0.5 (Beichman *et al.* 1984). The detection probability of the unassociated IRAS sources except the cirri is less than 2 in our survey region.

Table A2 shows the list of all the IRAS sources in the survey regions, together with classification and identification to the NIR sources. There are 8 PMS candidates

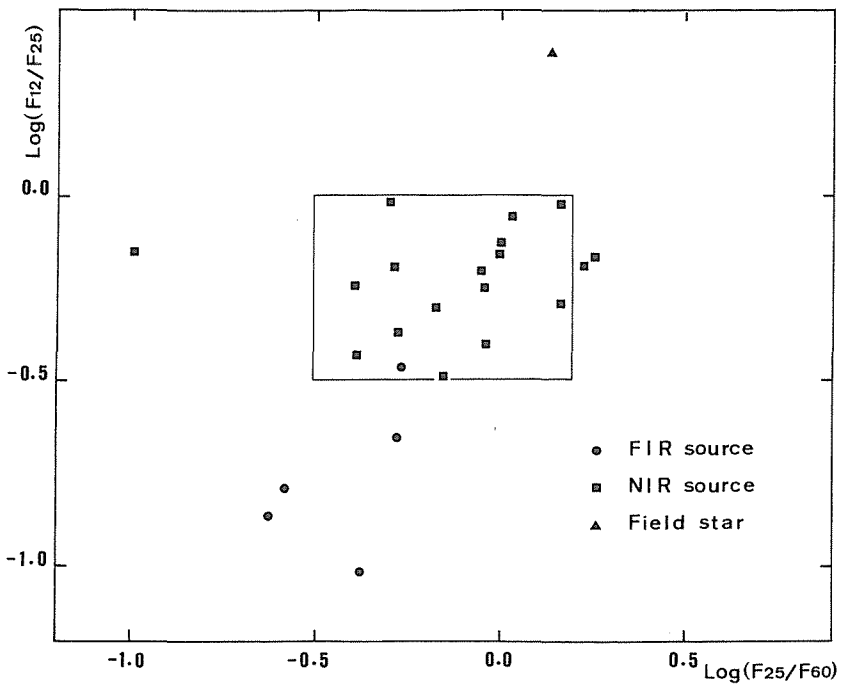

Figure 4 Two-color diagram of ([12]–[25], [25]–[60]) for the IRAS sources detected in the survey regions.

not identified to the NIR sources. They could be heavily obscured younger objects staying still in the dense region, namely, embedded TTSs or proto-stars (Beichman *et al.* 1986).

5. Mass of the cloud and efficiency of the star formation

5.1. Mass of the cloud derived by using the field stars

As mentioned in Sect. 4.2, the majority of the sources detected in the NIR survey are field stars. These field stars can be used to derive the cloud mass through the extinction undergone to them, assuming both the wavelength dependence of the selective extinction and the gas-to-dust ratio.

First, it is necessary to exclude foreground field stars from the group of field stars. If a star is located in front of the cloud, it is not reddened by the cloud at all. The amount of interstellar reddening between the cloud and the earth is very small and negligible compared to the reddening within the dark cloud; the (J–K) excess caused by the interstellar reddening is less than 0.1 mag at the distance of 140 pc. Therefore, they can be easily distinguished from background stars by their smaller color excess than that of the latter. The objects whose visual extinction in Table A1 is smaller than 1.0 mag have been regarded as foreground stars, and we will pay no more attention hereafter.

We will use the background stars located behind the cloud so as to evaluate the extinction caused by the cloud, and delineate the spatial distribution of the extinction over the cloud. The visual extinction A_v of an individual sources can be derived from the following relation:

$$A_v = 5.7 \times E(\mathrm{J-K}) \qquad \text{(Koornneef 1983)},$$

where the color excess E(J–K) is defined as subtraction of intrinsic color from observed color, $(\mathrm{J-K})_o - (\mathrm{J-K})_i$. Because of the lack of spectroscopic data, the approximate value of the intrinsic color were obtained by backing the observed color along a reddening trajectory until it came across the intrinsic color locus. The results of this procedure applied to the individual background stars are given in column 9 of Table A1. From these, the contour maps of the visual extinction can be constructed for the survey region. In drawing the contour we also made reference to the contour map of the integrated ^{13}CO (J=1→0) intensity (Kleiner and Dickman 1984) and visual extinction map by star counts (Cernicharo, Bachiller and Duvert 1985). Plate 1, 2, and 3 show the contour maps, and average extinction within the contour.

The hydrogen column density corresponding to the visual extinction is obtained by the relation.

$$\mathrm{N(H)} = 1.2 \times 10^{21} \times A_v \ \mathrm{cm}^{-2} \qquad \text{(Dickman 1978)},$$

and a partial mass within a contour is calculated by multiplying the column density by the partial area. Thus we have obtained the total mass of 330, 190, and 390 $M_\odot$ for the region 1, 2, and 3, respectively.

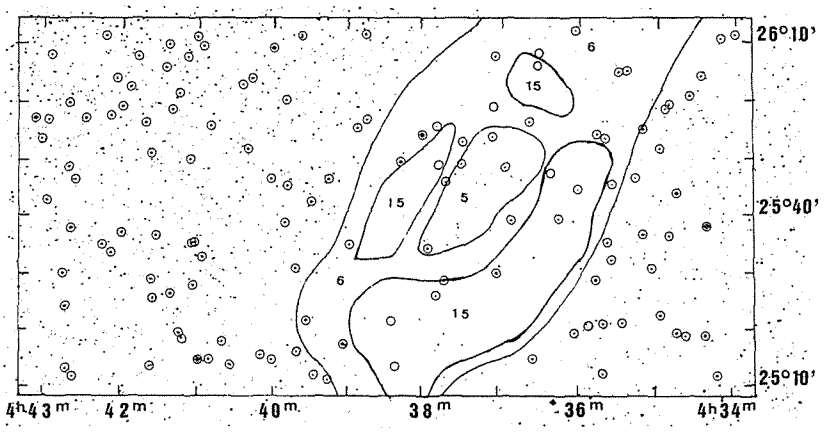

Plate 1. The spatial distribution of the NIR sources in the region 1. The numeral is an average of visual extinction in a contour, obtained from that of the background field stars (see Sect. 5.1).

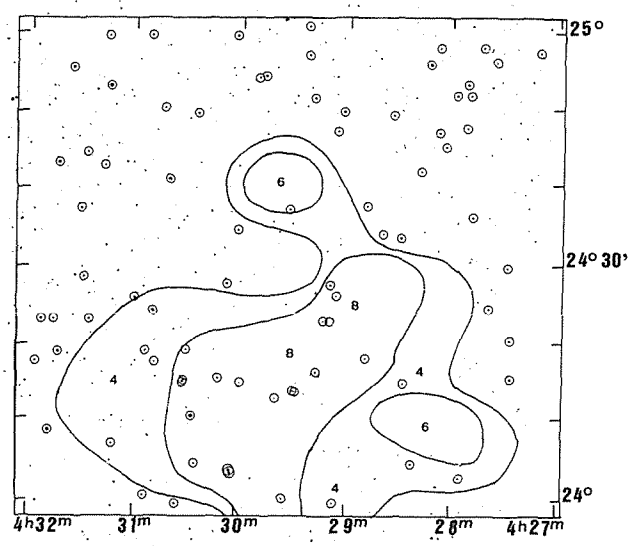

Plate 2. Same as Plate 1 but region 2.

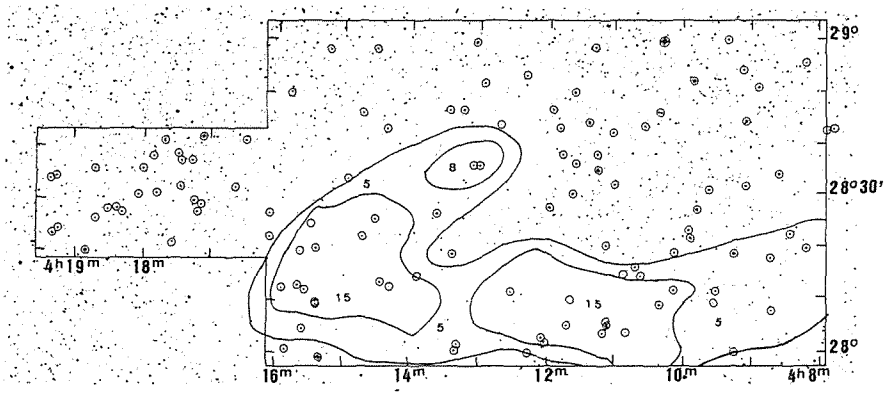

Plate 3. Same as Plate 1 but region 3.

5.2. Star formation efficiency in the dark cloud

An important purpose of the present study is to determine the efficiency of star formation, that is, the fraction of the matter that is converted into stars in a region. In the previous sections, we have identivied PMS objects of various kinds and estimated the cloud mass for each survey region. Cohen and Kuhi (1971) showed the H–R diagrams for the optical PMS objects together with stellar evolution tracks for given masses. In the Taurus region, the mean mass of them is about 0.8 $M_{\odot}$. If we adopt the mean value for the all PMS objects in our survey regions, the total stellar masses in the region 1, 2, and 3 are 16.0, 12.8, and 20.8 $M_{\odot}$, respectively. The star formation efficiency can be evaluated by division of the total stellar mass by the cloud mass. Consequently, the values of 4.8, 6.8, and 5.3% are obtained for the region 1, 2, and 3, respectively.

Cohen and Kuhi (1979) roughly estimated the efficiency, ranging between 2% and 9% in the several dense regions. Although the methods of the estimation are different, our results are not inconsistent with them. If we take only optically known members into account, the efficiency in the region 1 will be far smaller than that in the region 2 because the region 1 contains larger mass and less optical PMS objects than the region 2. Our results, however, indicate that the efficiency is similar in the three regions, which may suggest that the star formation occurred independently and almost concurrently in the several regions of the complex.

6. Discussion

6.1. Is our survey deep enough to reveal the embedded objects?

The limiting magnitude guaranteeing the completeness of the survey is an important factor in judging whether the survey is capable of picking up a substantial fraction of the embedded objects or not. In order to find out the majority of the embedded objects, the survey system should be sensitive enough to detect the objects whose magnitudes are fainter than that at the peak in the luminosity function. Jones and Herbig (1979) presented a luminosity function model of TTSs in terms of K magnitude. It was constructed on the basis of the optically known TTSs within the Taurus-Auriga dark cloud complex (Rydgren, Strom and Strom 1976; Cohen and Kuhi 1979), which peaks in the range of 8.0 mag–8.5 mag. The NIR survey in the Taurus complex by Elias (1978c) is not deep enough to reveal the PMS objects because of the low limiting magnitude, about 7.5 mga in the K band. According to the model, only 25% of the TTSs could be detected in Elias' survey. On the other hand, the limiting magnitude of the present survey in the K band is 9.5 mag. The model predicts that about 95% of the TTSs are brighter than our limiting magnitude. If we assume that the luminosity function of PMS objects is similar to that of TTSs in our survey regions, it can be said almost all the PMS objects have been detected in our survey. In fact all of the known PMS objects in the survey regions were detected.

However, one must recognize that the obscuration by intracloud matter or circumstellar matter reduces the apparent magnitudes of PMS objects. The visual extinction,

listed in Table A1 for the field stars, exceeds 10 mag in heavily obscured regions, in some cases as much as 20 mag. Although the extinction in the K band is about one tenth of the visual extinction, our limiting magnitude is insufficient to detect the PMS objects in such regions. If we adopt a mean value of the extinction in the K band as 1.5 mag in such regions, which reduces the limiting magnitude to 8.0 mag apparently, only 43% of the PMS objects may be detected in the present survey. We may have to leave the remaining embedded objects to longer wavelength observations. Fortunately, since the IRAS survey is available (see Sect. 4.3), we can pick up the embedded objects in locally obscured areas in the cloud. So far as they have considerable excess in the FIR range, they must be detected in the IRAS survey.

6.2. The remaining association members

In order to estimate the star formation efficiency in a cloud strictly, it is clear that one should find out all kinds of the association members which are born in the cloud. Although all means of investigations including the present work have been carried out in order to find out the PMS objects, some kinds of association members may remain not identified yet in the survey regions. Hereafter, we will discuss the possible remaining association members: obscured WELSs and evolved members that are born in the regions but have already evolved into ZAMS.

(a) The obscured weak emission line stars

As mentioned in Sect. 2, the WELSs are not conspicuous PMS objects, showing only faint emission lines. Since they scarcely show infrared excess (Mundt *et al.* 1983; Herbig, Vrba, and Rydgren 1986), they can not be discriminated from normal stars in the diagram of (J–H, H–K). If they are embedded in or located behind dense regions, it is hardly possible to find them. In order to estimate the numbers of the obscured WELSs we would adopt three assumption as the following. Firstly, the ratio of the TTSs to the WELSs is constant everywhere in the Taurus complex. We obtained the ratio of 28 to 7 from the optical PMS objects in the survey regions. Secondly, all the newly identified PMS candidates in the present work are TTSs. Thirdly, the investigations to detect the TTSs and the WELSs were made completely to the same level of the obscuration. An extrapolation under these assumptions suggests that 7 WELSs remain undetected yet in the survey regions. Of them 5 objects belong to the region 1 and the rest belong to the region 3. They will increase the efficiency by 1.2% and 0.3% for the region 1 and region 3 respectively.

(b) The evolved association members

We have considered only the population of PMS objects in the estimation of the star formation efficiency so far, but we should consider the population of evolved members also. Since they have already evolved into ZAMS, it is fundamentally impossible to discriminate them from the field stars. Thus in order to estimate their effect in the efficiency, one can not but guess the amount of them in the viewpoint of cloud evolution. If the star formation has proceeded over one or more Kelvin-Helmholtz contraction times, their existence will give rise to a serious problem in the

estimation of the efficiency.

Fortunately, it seems plausible that there are no evolved stars in the Taurus cloud complex. Cohen and Kuhi (1979) discussed the age of the PMS objects and concluded that the upper limit to the ages in this complex is 6×10^6 years and the majority are younger than 1.6×10^6 years. The age distribution of the WELSs (Fig. 2 in Herbig, Vrba and Rydgren 1986) confirmed the conclusion. Various observations were carried out in order to discover the post-TTSs in this complex but ended in failure (Sect. 3.1). Lindroos (1986) made it clear that almost all the post-TTSs identified in a investigation of binary stars still show CaII emission and strong Li absorption at an age of 50×10^6 years. If the post-TTSs existed in this complex, they would have been discovered. Thus we need not consider the existence of the evolved star of low mass. Incidentally, the upper limit (6×10^6 years) corresponds to the evolution time scale of about $2\,M_\odot$ stars to ZAMS (Fig. 7 in Cohen and Kuhi 1979). Meanwhile, this complex is also well-known as a birth place of only low-mass stars such as TTSs of less than $2\,M_\odot$. The evidence for the formation of low mass stars is very convincing, while no evidence for the formation of massive stars are found in radio and FIR observations (Gilmore 1980; Sargent *et al.* 1983; Gaida *et al.* 1984). Thus we conclude that the effect by evolved members is negligible in this complex.

6.3. A speculation upon the star formation in the Taurus complex

It appears to be plausible that the star formation in the Taurus complex started at 6 million years ago and continued since that time (Sect. 5.2; Fig. 2 in Herbig, Vrba and Rydgren 1986). However, it is unclear where the formation started from and whether the formation has continued up to the present or not.

As shown in Sect. 5.2, the star formation efficiency is virtually the same (about 5–6%) in the three regions although the optical appearances are very different in each region (see Sect. 3.1). We can elucidate it by the fact that the region 1 contains many embedded objects only visible in the infrared, while the region 2 contains many optical PMS objects. It is natural to consider that the embedded objects are generally younger than the optical objects. In this respect, the onset of star formation in the region 1 appears to be delayed compared with that in the region 2. The region 3 shows intermediate properties in every point. Probably, the star formation started in the region 2 at first, proceeded to the region 3, and onset in the region 1 later. However, it seems that each star formation was not triggered externally but initiated spontaneously and quiescently since there are no signs of H II region or supernova activities (Gilmore 1980).

The PMS objects appear to be capable of dissipating their placental cloud with stellar winds (Lada, Margulis and Dearborn 1984). Murphy and Myers (1985) discovered an expanding shell in Barnard 18 (the region 2) and showed that steller winds from PMS objects may have a sufficient momentum to drive the shell expansion. It appears that the stellar winds are disrupting the Barnard 18. As shown above, this cloud contains many optical PMS objects but only embedded PMS candidate, which may be caused by the dissipation. The residual gas in the region 2 seems to be being cleared up, after the phase of star formation. Probably the star formation has already

ceased in the region 2. In comparison with the region 2, the region 1 and 3 contain many embedded PMS candidates. Moreover, no evidence of dissipation has been discovered yet in the region 1 and 3. It is not certain whether the star formation in the regions has continued to date or already ended also. In the former case, the continuing star formation will increase the efficiency. However, since the regions have evolved under the same environment as the regions 2, we may expect that the efficiency should be about the same in the three regions. As shown above the efficiency is virtually the same in the three regions. Therefore, it can hardly be expected a large number of stars to be newly formed in the region 1 and 3. As the disruption proceeds, the mass in a given area will decrease. In other words, the disruption acts on raising the efficiency apparently. The small difference in the efficiency might reflect the difference in proceeding of dissipation.

In order to produce a gravitationally bound stellar system, the star formation efficiency should exceed either 50% in the case of rapid dissipation or 30% in the case of slow dissipation (Lada, Margulis and Dearborn 1984). Wilking and Lada (1983) discovered a population of embedded objects in the dense core of the ρ Ophiuchi dark cloud. Subsequently, Lada and Wilking (1984) obtained a high star formation efficiency, larger than 25%, and confirmed the suggestion that the ρ Ophiuchi cloud is a site of an embedded, young open cluster (Grasdalen, Strom and Strom 1973; Vrba *et al.* 1975). In comparison to the efficiency of the ρ Ophiuchi cloud our results in the dense regions of the Taurus complex are far smaller, although we have obtained it including all kinds of PMS objects. Probably the star formation in the Taurus complex would result in production of unbound stellar associations, although the individual members appear at present to be bound in the placental cloud (Jones and Herbig 1979).

Acknowledgements

I would like to express my sincere appreciation to Prof. H. Hasegawa and Dr. S. Sato for their kind instruction throughout the preparation of this thesis. Without their encouragements I would have accomplished a tiny portion of this thesis.

I am also deeply grateful to the group faculties begining with Dr. T. Maihara who have taught me what is the infrared astronomy. I would like to thank all group members, especially T. Nagata, T. Yamashita and M. Tamura, for their kind assistance in the observations and encouragement.

Finally, I wish to thank the staff members of the Kiso Observatory headed by Prof. K. Ishida for their hospitality and Dr. T. Ichikawa for his assistance in measurement of the source position.

References

Allen, D. A. 1972, Ap. J. (Letters), **172**, L55.

Beichman, C. A., et al. 1986, Ap. J., **307**, 337.

Beichman, C. A., Neugebauer, G., Habing, H. J., Clegg, P. E., and Chester, T. J. 1984, Infrared Astronomical Satellite, Catalogs and Atlases (Pasadena: Jet Propulsion Laboratory)

Cernicharo, J., Bachiller, R., and Duvert, G. 1985, Astr. Ap., **149**, 273.

Clark, F. O., Giguere, P. T., and Crutcher, R. M. 1977, Ap. J., **215**, 511.
Cohen, M., and Kuhi, L. V. 1979, Ap. J. Suppl., **41**, 743.
Dickman, R. L. 1978, Ap. J. Suppl., **37**, 407.
Elias, J. H. 1978a, Ap. J., **223**, 859.
Elias, J. H. 1978b, Ap. J., **224**, 453.
Elias, J. H. 1978c, Ap. J., **224**, 857.
Feigelson, E. D., and Kriss, G. A. 1981, Ap. J. (Letters), **248**, L35.
Feigelson, E. D., and Kriss, G. A. 1983, A. J., **88**, 431.
Gaida, M., Ungerechts, H., and Winnewisser, G. 1984, Astr. Ap., **137**, 17.
Gilmore, W. 1980a, A. J., **85**, 894.
Gilmore, W. 1980b, A. J., **85**, 912.
Grasdalen, G. L., Strom, K. M., and Strom, S. E. 1973, Ap. J. (Letters), **189**, L53.
Hayashi, C. 1961, Pub. Astr. Soc. Japan, **13**, 450.
Hayashi, C. 1966, Ann. Rev. Astr. Ap., **4**, 171.
Heiles, C. E. 1968, Ap. J., **151**, 919.
Herbig, G. H. 1977, Ap. J., **214**, 747.
Herbig, G. H. 1978, Problems of Physics and Evolution of the Universe, edited by L. V. Mirzoyan (Yerevan; House of American Academy of Sciences), p. 171.
Herbig, G. H., and Rao, N. K. 1972, Ap. J., **174**, 401.
Herbig, G. H., Vrba, G. H., and Rydgren, A. E. 1986, A. J., **91**, 575.
Hyland, A. R. 1980, Infrared Astronomy, IAU Symp. No. **96**, edited by C. D. Wynn-Williams and D. P. Cruikshank (Reidel, Dordrecht, Holland), p. 125.
Hyland, A. R., Jones, T. J., and Mitchell, R. M. 1982, M. N. R. A. S., **201**, 1095.
Jones, B. F., and Herbig, G. H. 1979, A. J., **84**, 1872.
Jones, T. J., Ashley, M., Hyland, A. R., and Ruelas-Mayorga, A. 1981, M.N.R.A.S., **197**, 413.
Jones, T. J., and Hyland, A. R. 1980, M.N.R.A.S., **192**, 359.
Koornneef, J. 1983, Astr. Ap., **128**, 84.
Kleiner, S. C., and Dickman, R. L. 1984, Ap. J., **286**, 255.
Lada, C. J., Margulis, M., and Dearborn, D. 1984, Ap. J., **285**, 141.
Lada, C. J., and Wilking, B. A. 1984, Ap. J., **287**, 610.
Lindroos, K. P. 1986, Astro. Ap., **156**, 223.
Mendoza V., E. E. 1966, Ap. J., **143**, 1010.
Mendoza V., E. E. 1968, Ap. J., **151**, 977.
Mundt, R., Walter, F. M., Feigelson, E. D., Finkenzeller, U., Herbig, G. H., and Odell, A. P. 1983, Ap. J., **269**, 229.
Murphy, D. C., and Myers, P. C. 1985, Ap. J., **298**, 818.
Myers, P. C., and Bension, P. J. 1983, Ap. J., **266**, 309.
Myers, P. C., Fuller, G. A., Mathieu, R. D., Beichman, C. A., Benson, P. J., Schild, R. E., and Emerson, J. P. 1987, Ap. J., **319**, 340.
Myers, P. C., Linke, R. A., and Bension, P. J. 1983, Ap. J., **264**, 517.
Nakajima, T., Nagata, T., Nishida, M., Sato, S., and Kawara, K. 1986, M.N.R.A.S., **221**, 483.
Neugebauer, G., et al. 1984, Ap. J. (Letters), **278**, L1.
Rucinski, S. M. 1985, A. J., **90**, 2321.
Sargent, A. I., van Duinen, R. J., Nordth, H. L., Friedlund, C. V. M., Aalders, J. W. G., and Beintema, D. 1983, A. J., **88**, 88.
Rydgren, A. E., Schmelz, J. T., and Vrba, F. J. 1982, Ap. J., **256**, 168.
Rydgren, A. E., Strom, S. E., and Strom, K. M. 1976, Ap. J. Suppl., **30**, 307.
Rydgren, A. E., and Vrba, F. J. 1983, A. J., **88**, 1017.
Strom, K. M., Strom, S. E., and Vrba, F. J. 1976, A. J., **81**, 308.
Vrba, F. J., Rydgren, A. E. 1985, A. J., **90**, 1490.
Vrba, F. J., Strom, K. M., Strom, S. E., and Grasdalen, G. L. 1975, Ap. J., **197**, 77.
Walter, F. M., and Kuhi, L. V. 1981, Ap. J., **250**, 254.

Weaver, W. B. 1983, M.N.R.A.S., **205**, 389.
Wilking, B. A., and Lada, C. J. 1983, Ap. J., **274**, 698.

Appendix 1. Observational data for the sources detected in the survey

The data of the sources detected in each region are given in Table A1-1, 2, and 3 with the following contents:

Column 1: Source number arranged in order of right ascension.

Column 2 and 3: Equatorial coordinate (R. A. and Dec.).

Column 4 to 6: Photometric magnitudes in the J, H, and K band.

Column 7 and 8: Colors of (J-H) and (H-K).

Column 9: Visual extinction for a field star/ Attribute for a PMS object. W: WELS, T: TTS N: PMS candidate identified in NIR, F: PMS candidate identified in FIR.

Column 10: Identification with our candidates or previously- known objects. K: Kim (this paper) S: SAO Catalog, E: Elias (1978c), HK Tau/G: Cohen and Kuhi (1979), FK: Feigelson and Kriss (1981), LK CaII: Herbig, Vrba, and Rydgren (1986).

Table A1-1. Near-infrared sources detected in the region 1.

No.	R.A.(1950)	Dec.(1950)	J	H	K	J-H	H-K	Av/At	Id.
1	$4^h34^m\ 0.1^s$	26°10'56"	10.19	9.41	9.01	0.78	0.40	N	K
2	4 34 11.2	26 10 16	10.05	8.66	8.21	1.38	0.45	5.9	
3	4 34 12.1	25 11 31	8.36	7.28	6.93	1.08	0.36	3.6	E 29
4	4 34 20.9	25 37 40	5.14	4.50	4.32	0.64	0.18	0.1	S 76676
5	4 34 21.2	25 18 32	7.19	6.05	5.69	1.14	0.36	4.0	
6	4 34 23.9	26 4 30	9.19	7.43	6.76	1.75	0.67	9.3	
7	4 34 28.5	26 1 13	8.52	7.58	7.21	0.94	0.36	2.9	
8	4 34 34.6	25 17 1	9.89	9.39	9.30	0.49	0.09	0.0	
9	4 34 43.6	25 19 1	8.93	7.74	7.13	1.19	0.61	N	K
10	4 34 44.4	25 43 29	5.08	3.61	3.07	1.46	0.54	5.2	
11	4 34 50.1	25 36 0	10.57	9.59	9.30	0.97	0.29	2.7	
12	4 34 51.1	25 58 57	11.04	10.12	9.85	0.92	0.27	2.3	
13	4 34 54.2	25 58 13	10.04	8.90	8.48	1.14	0.41	4.3	
14	4 34 55.0	25 51 15	9.80	8.73	8.30	1.07	0.43	4.0	
15	4 34 56.5	25 22 11	7.00	5.71	5.24	1.29	0.46	5.5	
16	4 35 3.3	25 30 21	10.96	10.20	9.95	0.75	0.25	1.2	
17	4 35 11.0	25 36 16	8.39	7.31	6.97	1.08	0.35	3.6	
18	4 35 11.2	25 54 40	8.84	8.39	8.19	0.45	0.20	2.4	
19	4 35 17.0	25 46 7	10.29	8.89	8.21	1.40	0.68	N	K
20	4 35 24.2	26 4 55	9.55	8.37	7.50	1.19	0.87	TNF	DO Tau
21	4 35 26.6	25 21 0	9.83	8.79	8.42	1.04	0.37	3.5	
22	4 35 30.9	26 4 45	9.25	8.30	7.91	0.94	0.39	3.1	
23	4 35 35.4	25 45 12	11.22	9.77	9.22	1.45	0.54	6.9	
24	4 35 35.5	25 31 59	11.24	10.44	10.02	0.81	0.41	N	K
25	4 35 39.0	25 35 1	10.32	9.63	9.29	0.69	0.34	1.3	
26	4 35 41.0	25 53 11	10.93	9.98	9.57	0.95	0.41	3.2	
27	4 35 41.4	25 20 51	9.78	8.67	8.30	1.11	0.37	4.0	
28	4 35 41.5	25 12 7	9.93	8.64	8.21	1.29	0.43	5.3	
29	4 35 47.4	25 53 51	9.24	7.93	7.44	1.31	0.49	5.7	
30	4 35 47.9	25 28 24	6.70	5.38	4.94	1.32	0.44	5.5	
31	4 35 52.7	25 20 18	11.44	10.33	9.81	1.11	0.52	N	K
32	4 36 2.0	25 44 16	10.88	9.01	8.24	1.87	0.77	10.5	
33	4 36 3.7	25 19 12	11.10	9.82	9.36	1.18	0.46	4.9	
34	4 36 4.8	26 11 54	10.52	8.94	8.31	1.58	0.63	8.1	
35	4 36 17.1	25 39 12	10.34	8.93	8.14	1.41	0.79	N	K
36	4 36 22.8	25 47 9	11.16	8.26	6.94	2.90	1.32	19.6	E 15
37	4 36 33.3	26 8 7	11.86	10.38	9.78	1.48	0.60	7.4	
38	4 36 34.0	26 5 50	10.70	7.02	5.12	3.68	1.90	27.4	E 16
39	4 36 36.7	25 14 44	9.60	9.08	8.80	0.52	0.28	3.9	
40	4 36 43.2	25 55 52	10.74	9.64	9.12	1.09	0.53	N	K
41	4 36 53.0	25 39 30	10.52	7.93	6.04	2.59	1.89	NF	E 18

42	4	36	59.5	25	48	7	9.92	8.55	7.96	1.37	0.60	6.7	
43	4	37	5.4	25	29	45	8.33	7.66	7.47	0.67	0.19	0.3	
44	4	37	6.0	25	59	53	12.31	10.43	9.18	1.87	1.25	NF	K
45	4	37	7.8	26	7	33	9.89	8.80	8.40	1.09	0.41	4.0	
46	4	37	9.6	25	53	30	10.03	8.23	7.50	1.80	0.74	9.9	
47	4	37	32.8	25	52	33	10.31	8.98	8.43	1.34	0.54	6.2	
48	4	37	34.2	25	48	42	10.63	9.54	9.12	1.09	0.42	4.1	
49	4	37	42.2	25	26	10	12.14	10.22	9.39	1.92	0.82	11.2	
50	4	37	45.5	25	45	35	10.74	9.94	9.49	0.80	0.46	N	K
51	4	37	46.1	25	28	21	9.69	9.20	9.04	0.49	0.16	1.0	
52	4	37	52.1	25	25	51	9.65	7.94	7.27	1.72	0.67	9.1	
53	4	37	52.6	25	55	20	11.38	9.55	8.83	1.84	0.72	10.1	
54	4	37	53.0	25	48	57	13.09	9.22	7.44	3.87	1.78	27.8	
55	4	37	58.9	25	34	3	6.66	5.76	5.23	0.89	0.54	N	K
56	4	38	3.7	25	53	50	5.94	5.55	5.32	0.39	0.24	F	S 76704
57	4	38	20.5	25	49	6	7.05	6.50	6.18	0.56	0.32	0.4	
58	4	38	25.9	25	13	39	12.30	10.38	9.55	1.92	0.83	11.2	
59	4	38	26.6	25	21	20	10.67	8.57	7.68	2.10	0.89	12.6	
60	4	38	46.8	25	56	29	11.01	9.85	9.45	1.16	0.41	4.4	
61	4	38	48.3	26	11	18	10.48	9.97	9.74	0.51	0.22	2.6	
62	4	38	53.7	25	55	3	9.28	8.07	7.62	1.21	0.45	4.9	
63	4	38	59.5	25	34	47	10.35	9.34	8.97	1.00	0.38	3.3	
64	4	39	4.2	25	17	32	8.92	7.73	7.11	1.19	0.62	TNF	Lk Hα 332
65	4	39	15.1	25	11	15	10.24	9.08	8.65	1.15	0.43	4.5	
66	4	39	15.8	25	46	9	9.17	8.87	8.67	0.30	0.20	3.4	
67	4	39	25.9	25	12	5	10.68	9.34	8.88	1.34	0.45	5.7	
68	4	39	29.3	25	42	15	8.30	7.45	7.16	0.85	0.29	2.0	
69	4	39	32.1	25	21	37	7.47	6.06	5.56	1.40	0.51	6.4	
70	4	39	37.6	26	10	57	9.89	9.09	8.88	0.80	0.20	1.2	
71	4	39	39.7	25	16	12	10.40	9.41	9.02	0.99	0.39	3.3	
72	4	39	40.7	25	30	41	9.14	8.38	8.11	0.76	0.28	1.4	
73	4	39	48.4	25	45	5	10.09	9.71	9.58	0.38	0.13	1.0	
74	4	39	49.9	25	38	41	9.72	8.91	8.66	0.82	0.24	1.5	
75	4	39	50.1	25	59	57	10.06	9.70	9.53	0.36	0.18	2.3	
76	4	39	58.9	25	14	40	10.75	9.90	9.52	0.85	0.38	TN	GO Tau
77	4	39	59.5	25	46	53	10.54	9.78	9.52	0.77	0.26	1.3	
78	4	40	0.3	26	8	58	5.89	5.18	5.00	0.71	0.18	0.5	S 76725
79	4	40	9.1	25	15	28	10.72	9.41	9.00	1.30	0.41	5.2	
80	4	40	17.3	26	3	45	9.64	8.74	8.48	0.90	0.26	2.0	
81	4	40	20.7	25	51	30	9.48	8.80	8.61	0.68	0.19	0.4	
82	4	40	24.8	26	2	44	10.83	10.16	9.93	0.67	0.23	0.5	
83	4	40	32.1	25	13	47	9.50	8.63	8.32	0.87	0.31	2.2	
84	4	40	39.8	25	17	52	8.92	7.73	7.35	1.19	0.38	4.4	
85	4	40	49.9	25	55	29	9.30	8.42	8.17	0.88	0.25	1.9	
86	4	40	51.2	25	14	54	9.68	9.25	9.04	0.42	0.22	3.0	
87	4	40	56.3	26	9	21	9.78	8.93	8.77	0.84	0.16	1.2	
88	4	40	58.2	25	14	42	3.33	2.09	1.60	1.24	0.49	5.4	IRC 30092
89	4	41	1.0	25	32	26	9.80	9.49	9.24	0.31	0.25	4.6	
90	4	41	1.6	26	11	0	9.99	9.36	9.13	0.62	0.24	0.4	
91	4	41	2.0	25	35	7	8.42	7.56	7.34	0.86	0.22	1.6	
92	4	41	3.3	25	27	38	8.53	7.38	7.00	1.15	0.37	4.1	
93	4	41	4.8	25	35	3	7.81	7.11	6.94	0.70	0.17	0.4	
94	4	41	6.8	25	49	42	9.11	8.02	7.70	1.08	0.33	3.5	
95	4	41	8.2	26	8	45	10.73	10.11	9.92	0.63	0.19	0.1	
96	4	41	12.1	25	18	30	9.81	9.45	9.29	0.36	0.16	1.9	
97	4	41	14.3	25	19	21	7.77	6.53	6.07	1.23	0.46	5.1	E 19
98	4	41	15.0	25	25	34	8.01	7.82	7.70	0.20	0.12	2.0	
99	4	41	17.5	26	0	18	9.96	9.22	9.01	0.74	0.21	0.9	
100	4	41	20.8	25	58	18	9.96	9.43	9.32	0.53	0.12	0.0	
101	4	41	23.8	26	9	36	9.78	9.24	9.03	0.54	0.21	1.8	
102	4	41	26.5	26	5	39	10.40	10.04	9.89	0.37	0.15	1.4	
103	4	41	32.8	25	36	21	9.70	9.45	9.28	0.25	0.17	2.8	
104	4	41	36.7	25	13	33	9.76	8.63	8.27	1.13	0.36	4.0	
105	4	41	36.9	25	28	46	10.13	9.78	9.54	0.35	0.24	4.1	
106	4	41	37.1	25	24	31	10.19	9.72	9.55	0.47	0.17	1.3	
107	4	41	37.4	25	50	41	8.99	8.77	8.60	0.21	0.17	3.2	
108	4	41	41.4	25	56	2	8.40	7.42	7.16	0.98	0.26	2.5	
109	4	41	48.3	26	7	30	10.55	10.19	10.05	0.36	0.14	1.2	
110	4	41	53.9	26	2	16	8.15	7.46	7.27	0.69	0.19	0.4	
111	4	41	59.4	25	36	50	10.38	9.93	9.62	0.45	0.31	5.4	
112	4	42	0.2	25	58	53	8.65	7.79	7.55	0.86	0.24	1.7	
113	4	42	4.1	26	3	44	10.45	9.85	9.63	0.60	0.22	0.1	

114	4 42 7.8	25 33 22	9.32	8.59	8.36	0.73	0.23	0.9			
115	4 42 8.9	25 57 16	9.80	9.43	9.29	0.37	0.15	1.5			
116	4 42 13.1	26 11 11	9.19	8.58	8.41	0.61	0.17	0.5			
117	4 42 14.7	25 34 48	9.30	8.58	8.38	0.72	0.20	0.7			
118	4 42 28.3	25 56 43	8.77	8.13	7.92	0.64	0.21	0.3			
119	4 42 35.7	25 46 3	10.49	9.90	9.74	0.59	0.16	0.3			
120	4 42 36.3	25 11 40	10.26	8.99	8.56	1.27	0.43	5.2			
121	4 42 38.9	25 37 34	8.68	8.35	8.25	0.33	0.10	0.5			
122	4 42 40.7	25 48 17	8.83	8.11	7.90	0.72	0.21	0.7			
123	4 42 41.1	25 59 23	9.12	8.41	8.18	0.71	0.23	0.8			
124	4 42 41.6	25 13 9	9.91	9.11	8.85	0.81	0.25	1.5			
125	4 42 42.4	25 23 59	7.52	6.80	6.58	0.72	0.21	0.8			
126	4 42 44.7	25 29 46	9.22	8.57	8.39	0.65	0.19	0.2			
127	4 42 55.4	26 7 54	10.92	10.33	10.01	0.59	0.32	0.6			
128	4 42 56.9	25 56 31	10.46	9.74	9.53	0.72	0.21	0.7			
129	4 42 57.6	25 42 29	9.03	8.38	8.16	0.65	0.22	0.4			
130	4 43 1.9	25 53 14	10.38	9.51	9.29	0.87	0.22	1.6			
131	4 43 7.5	25 56 48	6.90	6.85	6.83	0.05	0.02	0.2	S 76740		

Table A1-2. Near-infrared sources detected in the region 2.

No.	R.A.(1950)	Dec.(1950)	J	H	K	J-H	H-K	Av/At	Id.
1	$4^h27^m\ 2.7^s$	24°58'20"	10.15	9.49	9.21	0.66	0.28	0.8	
2	4 27 27.8	24 15 21	8.87	7.90	7.52	0.98	0.38	3.2	
3	4 27 27.9	24 20 17	9.58	8.55	8.01	1.03	0.54	TNF	FX Tau
4	4 27 29.8	24 29 33	10.77	9.86	9.56	0.91	0.31	2.4	
5	4 27 39.8	24 24 15	10.42	9.79	9.47	0.64	0.32	0.9	
6	4 27 44.9	24 56 51	10.63	9.90	9.73	0.73	0.17	0.6	
7	4 27 47.8	24 58 39	9.40	8.59	8.39	0.80	0.20	1.2	
8	4 27 49.4	24 35 56	9.52	8.74	8.40	0.78	0.33	TNF	ZZ Tau
9	4 27 51.3	24 51 25	10.22	9.86	9.74	0.36	0.12	0.8	
10	4 27 52.8	24 52 53	10.30	9.92	9.77	0.38	0.15	1.5	
11	4 27 53.1	24 47 20	10.98	10.27	10.02	0.72	0.24	0.9	
12	4 27 55.1	24 2 42	10.31	9.01	8.49	1.31	0.52	5.9	
13	4 27 58.9	24 51 33	9.92	9.28	9.10	0.64	0.17	0.1	
14	4 28 5.0	24 44 55	10.45	9.72	9.50	0.72	0.23	0.9	
15	4 28 8.9	24 46 44	10.47	9.88	9.70	0.59	0.18	0.9	
16	4 28 9.7	24 58 9	10.38	9.76	9.55	0.62	0.21	0.2	
17	4 28 14.1	24 55 25	7.19	6.80	6.72	0.39	0.08	0.0	S 76637
18	4 28 18.5	24 41 48	10.20	9.12	8.76	1.09	0.36	3.7	
19	4 28 22.4	24 4 28	9.87	9.01	8.70	0.86	0.31	W	Lk Hα 331
20	4 28 27.8	24 14 43	10.95	10.17	9.75	0.78	0.42	2.3	
21	4 28 29.6	24 33 19	8.11	6.92	6.52	1.19	0.40	4.5	
22	4 28 34.4	24 49 1	10.85	10.05	9.77	0.80	0.28	1.6	
23	4 28 39.3	24 34 17	10.89	9.50	8.98	1.39	0.52	6.4	
24	4 28 48.9	24 17 56	10.56	9.23	8.49	1.34	0.74	TNF	HK Tau
25	4 28 49.1	24 37 22	9.84	8.52	8.05	1.32	0.47	5.7	
26	4 29 2.8	24 49 24	8.47	7.74	7.52	0.73	0.22	0.8	
27	4 29 6.0	24 25 49	10.11	8.58	8.03	1.53	0.55	7.4	
28	4 29 6.6	24 46 53	11.02	10.47	10.19	0.55	0.27	0.1	
29	4 29 6.9	23 59 27	11.49	10.29	9.86	1.20	0.43	4.8	
30	4 29 9.6	24 27 17	7.77	6.13	5.51	1.64	0.61	8.4	E 9
31	4 29 11.3	24 22 20	13.10	9.99	8.11	3.11	1.88	N	K
32	4 29 13.6	24 22 39	10.32	8.58	7.55	1.74	1.03	TNF	E 23
33	4 29 17.2	24 16 8	9.45	8.40	8.03	1.05	0.38	W	HK Tau/G2
34	4 29 19.7	24 51 8	9.63	9.12	8.96	0.52	0.15	0.6	
35	4 29 23.1	24 56 32	10.31	9.98	9.82	0.33	0.16	2.0	
36	4 29 23.3	25 0 11	10.88	10.48	10.39	0.41	0.09	0.0	
37	4 29 28.9	24 13 38	10.12	8.99	8.23	1.13	0.76	TNF	FY Tau
38	4 29 30.1	24 13 44	9.93	8.64	7.64	1.29	1.00	TNF	FZ Tau
39	4 29 33.0	24 36 54	9.78	8.91	8.62	0.88	0.29	0.2	
40	4 29 35.4	24 0 1	10.79	9.77	9.47	1.02	0.30	3.0	
41	4 29 40.0	24 12 45	10.84	9.57	8.93	1.27	0.64	N	HK Tau/G1
42	4 29 47.7	24 53 57	8.98	8.26	8.10	0.71	0.16	0.4	
43	4 29 51.3	24 53 40	10.39	9.44	9.11	0.95	0.33	2.8	
44	4 30 0.3	24 14 43	11.01	10.20	9.77	0.81	0.43	2.5	
45	4 30 2.0	24 34 16	10.56	9.86	9.68	0.69	0.19	0.5	
46	4 30 3.8	24 58 59	8.89	8.12	7.91	0.77	0.21	1.1	

47	4	30	4.8	24	3	17	9.24	8.33	7.87	0.91	0.46	TNF	GH Tau
48	4	30	5.2	24	3	39	8.27	7.44	6.97	0.83	0.47	N	E 12
49	4	30	11.1	24	27	57	9.44	8.71	8.51	0.73	0.20	W	FK 3
50	4	30	12.7	24	15	20	9.66	8.57	8.18	1.09	0.39	3.9	
51	4	30	25.2	24	4	28	10.31	9.07	8.68	1.24	0.40	4.8	
52	4	30	25.4	24	49	7	10.00	9.79	9.71	0.22	0.08	0.7	
53	4	30	27.3	24	10	31	7.19	7.06	7.03	0.12	0.04	0.2	S 76651
54	4	30	30.5	24	18	57	9.90	8.63	8.20	1.27	0.43	5.1	
55	4	30	32.3	24	15	4	9.27	8.33	7.68	0.94	0.65	TNF	GI Tau
56	4	30	32.7	24	14	54	9.29	8.17	7.35	1.12	0.82	TNF	GK Tau
57	4	30	35.9	23	59	22	9.84	8.95	8.62	0.89	0.33	2.4	
58	4	30	40.9	24	40	44	7.82	6.98	6.73	0.84	0.25	1.7	
59	4	30	44.5	24	49	45	11.01	10.19	10.00	0.82	0.19	1.2	
60	4	30	48.6	24	17	20	11.38	10.40	10.04	0.98	0.37	3.1	
61	4	30	49.9	24	23	54	8.12	7.86	7.82	0.26	0.04	0.0	S 76653
62	4	30	52.3	24	58	58	10.14	9.33	9.10	0.81	0.23	1.4	
63	4	30	53.8	24	0	25	10.50	9.50	9.14	0.99	0.37	3.2	
64	4	30	53.8	24	18	47	10.21	9.40	9.16	0.81	0.24	1.4	
65	4	31	0.3	24	25	38	10.21	9.72	9.57	0.48	0.15	0.9	
66	4	31	12.1	24	6	53	11.19	10.20	9.89	1.00	0.30	2.9	
67	4	31	15.6	24	52	32	6.30	5.57	5.35	0.73	0.22	0.9	
68	4	31	16.5	24	58	54	10.90	9.99	9.75	0.91	0.24	2.0	
69	4	31	17.8	24	42	24	10.90	10.27	10.07	0.63	0.20	0.2	
70	4	31	26.2	24	22	45	8.77	7.72	7.38	1.05	0.33	3.3	
71	4	31	28.8	24	43	46	11.15	10.46	10.18	0.69	0.28	1.0	
72	4	31	29.4	24	28	12	9.38	8.45	8.20	0.93	0.25	2.1	
73	4	31	31.0	24	37	1	7.15	6.00	5.56	1.15	0.44	4.5	
74	4	31	36.7	24	54	50	8.52	7.97	7.85	0.55	0.13	0.0	
75	4	31	43.3	24	18	33	8.24	7.55	7.33	0.69	0.22	0.6	
76	4	31	44.0	24	42	44	7.29	6.22	5.93	1.08	0.29	3.2	
77	4	31	46.3	24	22	43	10.83	9.93	9.66	0.90	0.27	2.1	
78	4	31	48.5	24	8	31	7.52	7.31	7.17	0.20	0.14	2.4	S 76660
79	4	31	53.4	24	22	43	9.34	8.54	8.19	0.80	0.35	TNF	AA Tau
80	4	31	56.3	24	17	21	10.49	9.76	9.53	0.73	0.23	0.9	

Table A1-3. Near-infrared sources detected in the region 3.

No.	R.A.(1950)	Dec.(1950)	J	H	K	J-H	H-K	Av/At	Id.
1	$4^h\ 7^m 48.4^s$	28°43'01"	10.10	9.36	9.08	0.74	0.28	1.3	
2	4 7 52.2	28 42 18	10.88	9.63	9.24	1.24	0.39	4.8	
3	4 8 12.1	28 55 14	11.08	10.38	10.27	0.69	0.11	0.0	
4	4 8 12.1	28 19 23	8.69	7.59	7.23	1.10	0.36	3.8	
5	4 8 25.9	28 22 13	10.53	9.38	8.97	1.15	0.40	4.3	
6	4 8 35.9	28 33 45	8.04	6.84	6.39	1.20	0.44	4.9	
7	4 8 43.2	28 7 24	10.93	9.62	9.26	1.31	0.37	5.0	
8	4 8 43.7	28 17 33	9.67	8.64	8.23	1.03	0.41	3.7	
9	4 8 48.8	28 46 46	9.26	8.55	8.36	0.71	0.19	0.6	
10	4 8 54.1	28 50 40	9.61	9.05	8.99	0.56	0.06	0.0	
11	4 9 5.2	28 44 8	8.52	7.89	7.73	0.63	0.15	0.0	
12	4 9 5.6	28 31 36	10.02	9.40	9.27	0.62	0.13	0.0	
13	4 9 15.5	27 59 22	10.43	9.97	9.81	0.46	0.16	1.2	
14	4 9 15.6	28 18 27	8.33	8.08	7.93	0.24	0.16	2.6	S 76497
15	4 9 20.6	28 59 56	11.07	10.26	10.06	0.81	0.20	1.2	
16	4 9 31.6	28 11 22	10.76	9.68	9.39	1.08	0.28	3.3	
17	4 9 33.9	28 9 3	11.11	9.44	8.82	1.66	0.63	8.6	
18	4 9 37.8	28 31 00	9.02	8.30	8.11	0.71	0.20	0.6	
19	4 9 45.2	28 20 5	11.16	10.49	10.15	0.67	0.35	1.2	
20	4 9 48.9	28 27 14	9.77	9.05	8.90	0.72	0.16	0.4	
21	4 9 51.4	28 52 4	6.15	5.38	5.19	0.78	0.18	0.9	S 76503
22	4 9 53.7	28 21 39	7.92	7.07	6.79	0.86	0.27	1.9	
23	4 9 54.7	28 22 05	9.30	8.29	8.07	1.02	0.22	2.5	
24	4 10 8.4	28 18 50	10.22	9.26	8.68	0.96	0.58	WN	Lk CaII 1
25	4 10 8.4	28 11 34	9.70	8.90	8.68	0.80	0.22	1.3	
26	4 10 17.7	28 59 44	3.44	2.38	2.03	1.06	0.35	3.5	S 76508
27	4 10 19.7	28 45 59	10.18	9.44	9.28	0.74	0.16	0.6	
28	4 10 21.6	28 8 50	8.98	7.92	7.52	1.06	0.40	3.8	
29	4 10 34.5	28 43 19	10.63	9.88	9.72	0.75	0.16	0.6	

30	4	10	38.0	28	14	19	10.18	8.42	7.69	1.77	0.73	9.7	
31	4	10	42.9	28	16	9	8.68	7.26	6.65	1.42	0.61	7.0	
32	4	10	52.7	28	3	58	14.19	11.78	9.88	2.41	1.90	NF	K
33	4	10	53.3	28	14	44	11.45	10.20	9.68	1.25	0.52	5.6	
34	4	11	0.5	28	32	10	9.52	8.77	8.58	0.74	0.20	0.8	
35	4	11	2.4	28	42	10	9.48	8.34	8.06	1.14	0.29	3.6	
36	4	11	7.1	28	5	14	10.32	9.26	8.57	1.06	0.68	TN	FM Tau
37	4	11	7.3	28	4	41	7.60	6.76	6.42	0.83	0.34	W	HD 283447
38	4	11	8.6	28	20	26	9.51	8.69	8.29	0.82	0.40	TNF	FN Tau
39	4	11	11.3	28	3	20	9.70	8.17	6.98	1.53	1.19	TNF	CW Tau
40	4	11	15.8	28	34	55	5.15	3.98	3.52	1.18	0.45	4.8	
41	4	11	16.3	28	37	57	9.41	8.68	8.48	0.74	0.19	0.7	
42	4	11	17.8	28	58	38	9.71	8.82	8.58	0.88	0.25	1.9	
43	4	11	24.5	28	44	20	8.62	8.02	7.80	0.60	0.22	0.1	
44	4	11	35.6	28	36	15	10.07	9.84	9.64	0.23	0.20	3.9	
45	4	11	36.4	28	49	58	9.40	9.18	9.04	0.21	0.14	2.4	
46	4	11	38.6	28	9	53	12.16	9.49	8.09	2.67	1.40	18.8	
47	4	11	38.7	28	30	22	9.51	8.80	8.59	0.71	0.21	0.7	
48	4	11	43.7	28	5	0	9.70	8.77	8.19	0.93	0.58	TNF	FO Tau
49	4	11	47.4	28	38	2	9.79	9.06	8.79	0.74	0.27	1.2	
50	4	11	49.8	28	43	7	10.29	9.47	9.12	0.83	0.35	2.1	
51	4	11	55.8	28	46	38	10.29	9.57	9.37	0.72	0.19	0.7	
52	4	11	59.4	28	27	40	6.99	5.89	5.57	1.10	0.32	3.5	
53	4	12	3.4	28	1	46	9.96	9.31	9.07	0.64	0.25	0.5	
54	4	12	6.0	28	2	39	8.86	7.90	7.55	0.96	0.36	2.9	
55	4	12	18.4	27	59	40	10.68	9.74	9.24	0.94	0.50	N	K
56	4	12	19.7	28	53	20	10.50	9.73	9.50	0.77	0.22	1.1	
57	4	12	33.3	28	11	32	10.69	9.74	9.27	0.95	0.47	N	K
58	4	12	42.9	28	43	51	12.03	10.65	9.91	1.38	0.74	N	K
59	4	12	56.7	28	51	51	9.83	9.02	8.73	0.81	0.29	1.7	
60	4	13	0.8	28	36	1	8.94	7.89	7.56	1.04	0.33	3.3	
61	4	13	4.1	28	59	49	8.07	7.87	7.73	0.19	0.14	2.6	
62	4	13	6.5	28	36	4	11.20	10.20	9.83	1.00	0.37	3.3	
63	4	13	14.8	28	46	46	9.04	8.03	7.70	1.01	0.33	3.1	
64	4	13	20.3	28	1	20	10.42	9.04	8.57	1.38	0.47	6.0	
65	4	13	22.4	28	0	12	9.26	8.61	8.35	0.65	0.26	W	Lk CaII 4
66	4	13	24.9	28	18	51	8.47	7.65	7.35	0.82	0.30	1.8	
67	4	13	27.0	28	46	41	10.22	9.20	8.88	1.02	0.32	3.1	
68	4	13	38.4	28	26	42	8.72	7.94	7.64	0.78	0.30	1.6	
69	4	13	55.8	28	14	38	11.28	9.31	8.58	1.98	0.73	10.9	
70	4	14	19.6	28	12	30	10.57	9.80	9.43	0.77	0.37	2.0	
71	4	14	22.6	28	43	10	9.78	8.60	8.19	1.18	0.41	4.6	
72	4	14	27.7	28	13	27	9.78	9.06	8.62	0.73	0.43	TN	CY Tau
73	4	14	31.0	28	58	40	10.22	9.60	9.38	0.62	0.22	0.2	
74	4	14	32.6	28	25	41	10.40	9.66	9.37	0.74	0.29	W	Lk CaII 5
75	4	14	43.4	28	46	10	11.01	10.07	9.86	0.93	0.21	2.0	
76	4	14	43.5	28	22	17	11.54	10.07	9.22	1.47	0.85	N	K
77	4	14	59.2	28	34	41	11.26	10.35	9.87	0.91	0.48	N	K
78	4	15	21.6	27	58	54	4.66	3.83	3.56	0.82	0.28	1.7	
79	4	15	24.9	28	20	0	8.54	7.97	7.71	0.57	0.26	W	V410 Tau
80	4	15	25.5	28	9	7	9.42	8.43	7.77	1.00	0.66	TNF	DD Tau
81	4	15	25.6	28	9	43	10.60	9.73	9.24	0.87	0.49	TN	CZ Tau
82	4	15	26.0	28	24	00	12.84	10.74	8.91	2.10	1.83	NF	K
83	4	15	34.6	28	12	0	8.94	7.28	6.21	1.66	1.07	NF	E 1
84	4	15	36.5	28	4	26	10.39	9.62	9.26	0.76	0.36	1.9	
85	4	15	39.1	28	19	25	10.21	8.74	7.89	1.47	0.85	N	K
86	4	15	40.9	28	12	53	8.72	7.77	7.40	0.96	0.37	N	E 22
87	4	15	47.0	28	50	26	10.48	9.75	9.54	0.73	0.21	0.8	
88	4	15	51.9	28	0	36	10.39	9.51	9.18	0.89	0.33	2.4	
89	4	15	55.1	28	12	28	10.76	9.75	9.28	1.01	0.47	3.9	
90	4	16	6.5	28	22	20	10.98	10.31	9.83	0.67	0.48	TN	FQ Tau
91	4	16	6.5	28	26	53	10.99	10.20	9.88	0.79	0.32	1.7	
92	4	16	27.4	28	40	56	10.82	10.49	10.22	0.33	0.26	4.8	
93	4	16	49.9	28	35	33	9.74	9.11	8.91	0.63	0.21	0.2	
94	4	17	6.6	28	41	43	6.15	5.51	5.31	0.64	0.20	0.2	S 76556
95	4	17	11.4	28	29	10	10.06	9.65	9.46	0.41	0.19	2.3	
96	4	17	12.1	28	27	23	10.10	9.69	9.52	0.41	0.16	1.6	
97	4	17	14.3	28	29	19	8.29	7.65	7.47	0.64	0.17	0.1	
98	4	17	16.1	28	37	8	9.92	9.85	9.73	0.07	0.12	2.8	
99	4	17	25.6	28	37	3	9.29	8.44	8.20	0.85	0.24	1.7	
100	4	17	26.5	28	32	1	9.53	9.43	9.38	0.09	0.05	0.7	

101	4	17	28.4	28	38	16	9.60	8.70	8.45	0.90	0.25	2.0	
102	4	17	33.7	28	21	17	11.19	10.64	10.39	0.55	0.26	0.0	
103	4	17	40.9	28	41	0	9.75	8.80	8.53	0.95	0.27	2.4	
104	4	17	47.6	28	30	48	10.15	9.18	8.94	0.98	0.23	2.4	
105	4	17	50.3	28	38	1	10.07	9.40	9.23	0.68	0.16	0.2	
106	4	17	59.6	28	35	37	9.50	8.84	8.65	0.66	0.19	0.3	
107	4	18	3.8	28	30	31	9.77	8.96	8.75	0.81	0.21	1.3	
108	4	18	18.3	28	27	4	9.89	9.20	8.97	0.69	0.22	0.7	
109	4	18	22.7	28	27	49	8.69	7.62	7.28	1.07	0.34	3.5	
110	4	18	31.2	28	27	45	11.17	10.20	9.89	0.97	0.32	2.8	
111	4	18	42.2	28	25	53	10.18	8.83	8.31	1.35	0.52	6.1	
112	4	18	42.6	28	35	34	10.52	10.26	10.17	0.26	0.09	0.6	
113	4	18	50.8	28	19	35	7.35	6.16	5.25	1.19	0.91	TNF	RY Tau
114	4	19	16.1	28	23	40	9.21	8.32	7.99	0.89	0.33	2.4	
115	4	19	17.9	28	34	2	10.47	9.74	9.59	0.73	0.15	0.5	
116	4	19	20.1	28	22	58	8.62	7.47	7.15	1.15	0.32	3.8	
117	4	19	23.1	28	33	34	11.15	10.41	10.06	0.74	0.35	1.6	

Appendix 2. List of IRAS sources detected in our survey regions.

The data of the IRAS sources detected in each region are given in Table A2-1, 2, and 3 with the following contents:

Column 1: Source number arranged in order of right ascension.

Column 2 and 3: Equatorial coordinates (R.A. and Dec.).

Column 4 to 7: Flux densities (Jy) in the 12, 25, 60, and 100 μm band.

Column 8: Identification with the near-infrared sources.

Column 9: Attribute. W: WELS, T: TTS, N: PMS candidate identified in MIR, F: PMS candidate identified in FIR, S: Normal star, C: FIR cirrus.

Table A2-1. List of IRAS sources in the region 1.

No.	R.A(1950)	Dec(1950)	F(12)	F(25)	F(65)	F(100)	Id.	Att.
1	$4^h\ 34^m\ 19.9^s$	25° 37' 36"	0.90	<0.48	<0.40	<2.21	4	S
2	4 34 44.5	25 43 29	5.76	1.54	<0.40	<1.81	10	S
3	4 34 45.5	26 2 53	<0.25	<0.38	<0.40	3.01		C
4	4 34 53.1	25 50 32	<0.25	<0.48	<0.40	2.14		C
5	4 34 56.4	25 22 10	0.49	<0.34	<0.40	<9.95	15	S
6	4 35 23.9	26 4 51	1.91	3.89	5.84	6.30	20	TNF
7	4 35 41.1	25 16 39	<0.25	<0.32	<0.43	2.92		C
8	4 36 9.4	25 47 27	1.82	18.89	44.45	34.74		F
9	4 36 16.2	25 39 7	0.56	0.72	<0.40	<1.95	35	N
10	4 36 31.0	25 35 52	1.19	8.64	35.73	38.51		F
11	4 36 34.2	26 5 34	1.31	0.55	<0.40	<2.40	38	S
12	4 36 49.3	25 57 16	<0.25	0.75	17.58	72.18		F
13	4 36 54.6	25 39 17	5.21	6.81	7.16	17.74	41	NF
14	4 37 5.0	25 59 38	0.44	0.67	<0.40	<72.18	44	NF
15	4 37 59.3	25 34 2	0.47	<0.34	<0.40	<12.30	55	N
16	4 38 2.3	25 53 51	0.74	1.06	10.84	17.87	56	F
17	4 38 7.6	25 40 48	0.44	2.70	10.15	13.55		F
18	4 38 13.6	25 27 8	<0.25	<0.33	<0.40	3.01		C
19	4 38 34.2	25 50 43	0.54	1.55	2.83	<7.80		F
20	4 39 4.1	25 17 30	0.63	0.76	1.53	7.51	64	TNF
21	4 39 14.4	25 29 5	<0.29	<0.32	<0.40	2.80		C
22	4 39 31.8	25 21 37	0.38	<0.30	<0.41	<7.20	69	S
23	4 40 0.3	26 8 57	0.55	<0.39	<0.40	<5.52	78	S
24	4 41 2.9	26 4 5	<0.30	<0.45	<0.40	2.80		C
25	4 41 13.5	25 44 8	<0.25	<0.33	<0.40	0.40		C
26	4 41 23.8	26 8 33	<0.31	<0.31	0.81	<2.16		C
27	4 42 16.7	25 50 9	<0.25	<0.42	<0.40	3.16		C
28	4 42 58.7	25 20 6	<0.69	<0.75	<0.40	2.03		C
29	4 43 8.7	25 56 20	<0.25	<0.30	0.70	3.35	132	S

Table A2-2. List of IRAS sources in the region 2.

No.	R.A(1950)	Dec(1950)	12	25	65	100	Id.	Att.
1	$4^h\ 27^m\ 25.2^s$	24° 20' 7"	0.54	0.61	0.57	<6.73	3	TNF
3	4 27 50.6	24 35 24	0.77	1.33	3.31	4.19	8	TNF
4	4 28 35.1	24 37 3	<0.25	<0.32	<0.40	2.74		C
5	4 28 48.7	24 17 54	0.38	1.03	2.51	5.55	24	TNF
6	4 28 59.3	24 40 58	<0.25	<0.36	<0.40	3.37		C
7	4 29 13.2	24 22 39	1.06	3.98	7.05	9.54	32	TNF
8	4 29 13.6	24 27 26	<0.36	<0.25	<0.40	2.05		C
9	4 29 29.6	24 13 41	1.35	1.46	1.01	<2.80	38	TNF
10	4 30 4.7	24 3 28	0.57	0.97	1.05	<7.47	47	TNF
11	4 30 32.1	24 14 54	2.11	3.06	1.72	<6.92	56	TNF
12	4 31 16.1	24 52 34	0.42	<0.29	<0.40	<2.97	67	S
13	4 31 31.1	24 36 58	0.62	<0.48	<0.40	<2.84	73	S
14	4 31 53.5	24 22 44	0.39	0.61	1.20	<10.18	79	TNF

Table A2-3. List of IRAs sources in the region 3.

No.	R.A(1950)	Dec(1950)	12	25	65	100	Id.	Att.
1	$4^h\ 8^m\ 34.1^s$	28° 33' 42"	0.26	<0.42	<0.40	<4.68	6	S
2	4 9 45.3	28 8 58	<0.34	<0.27	<0.40	2.51		C
3	4 9 53.4	28 52 11	0.46	<0.30	<0.40	<8.08	21	S
4	4 10 17.6	28 59 46	8.60	2.02	<0.40	<6.75	26	S
5	4 10 49.3	28 3 58	0.87	3.88	7.38	10.57	32	NF
6	4 11 6.6	28 4 41	2.27	<2.82	<0.47	<10.57	36	TN
7	4 11 8.3	28 20 23	0.59	1.48	1.63	<6.03	38	TNF
8	4 11 15.5	28 3 35	2.26	3.61	3.24	<15.42	39	TNF
9	4 11 15.8	28 34 56	1.95	0.60	<0.40	<7.08	40	S
10	4 11 43.9	28 4 57	0.44	0.63	0.64	<7.19	48	TNF
11	4 12 6.7	28 29 19	<0.39	<0.25	0.78	2.13		F
12	4 13 33.6	28 43 29	<0.25	<0.51	<0.40	3.16		C
13	4 14 1.2	28 30 6	<0.25	<0.32	<0.40	3.50		C
14	4 15 20.3	27 58 52	2.12	<0.63	<0.40	<5.29	78	S
15	4 15 24.6	28 9 24	1.67	2.26	<1.54	<6.26	80	TNF
16	4 15 25.7	28 23 56	0.45	1.02	1.92	<7.55	82	NF
17	4 15 27.2	28 30 15	<0.42	<0.29	0.67	<8.53		C
18	4 15 34.8	28 15 1	33.20	99.90	72.38	166.10	83	NF
19	4 15 45.2	28 13 10	0.95	<4.50	<7.85	<70.00	86	N
20	4 15 51.8	28 5 9	<0.25	0.75	1.05	<7.29		F
21	4 18 36.4	28 26 14	<0.25	<0.44	<0.40	2.60		C
22	4 18 50.6	28 19 33	17.47	26.05	15.12	13.29	113	TNF